

Supporting information

Death and Rebirth: Photocatalytic Hydrogen Production by a Self-Organizing Copper-Iron System

Steffen Fischer,^{a,b} Dirk Hollmann,^b Stefanie Tschierlei,^c Michael Karnahl,^b Nils Rockstroh,^b Enrico Barsch,^{a,b} Patrick Schwarzbach,^c Shu-Ping Luo,^{b,d} Henrik Junge,^b Matthias Beller,^b Stefan Lochbrunner,^c Ralf Ludwig,^{a,b,*} and Angelika Brückner,^{b,*}

^a Institute of Chemistry, Department Physical Chemistry, University of Rostock, Dr. Lorenz-Weg 1, 18059 Rostock, Germany

^b Leibniz Institute for Catalysis at the University of Rostock, Albert Einstein-Straße 29A, 18059 Rostock, Germany

^c Institute of Physics, University of Rostock, Universitätsplatz 3, 18055 Rostock, Germany

^d State Key Laboratory Breeding Base of Green Chemistry-Synthesis Technology, Zhejiang University of Technology 310014 Hangzhou, China

* Corresponding author E-mail addresses: ralf.ludwig@uni-rostock.de and angelika.brueckner@catalysis.de

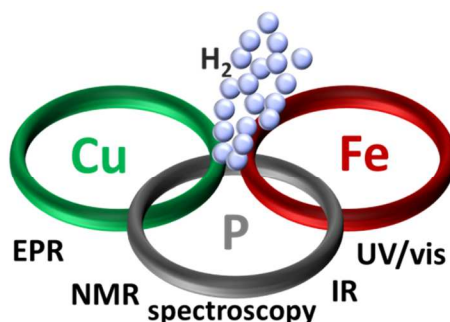


Table of contents:

Experimental details	page 2
UV/vis spectroelectrochemistry spectra of 1	page 5
Time-dependent absorption spectra of the photochemical reactions	page 6
DFT calculations of 1 , 1 ⁺ and 1 ²⁺	page 7
NMR measurements	page 8
IR spectra (measured)	page 9
IR spectra (calculated)	page 11
Photocatalytic experiments	page 12
References	page 13

Experimental details

In situ EPR spectra in X-band were recorded by a Bruker EMX CW micro spectrometer using an ER 4119HS-WI high sensitivity optical resonator with a grid in the front side. The temperature was adjusted by a Bruker Digital Temperature Control System ER4131VT. For irradiation with light, the beam of Xe-lamp (LOT-QuantumDesign, WLSB530) with a UV-Cut-Off-Filter (GG420, see www.lot-qd.com) was focused through the grid on the sample within the cavity. EPR measurements were performed at 300 K. For these measurements, 50 μl of a freshly prepared stock solution of **1** (7 mM) in THF/TEA (5/1) was filled in a 3 mm EPR tube under argon atmosphere. The g -values have been obtained from the resonance field B_0 and the resonance frequency ν using the resonance condition $h\nu = g\beta B_0$. The calibration of the g -values was performed using DPPH (2,2-diphenyl-1-picrylhydrazyl, $g = 2.0036 \pm 0.00004$) as standard. EPR spectra simulation was performed using the program Simfonia (Bruker).

EPR spectroelectrochemistry measurements were performed in a home-made electrochemistry EPR cell with a platinum mesh (round, $d=5$ mm) as working electrode, a platinum wire as counter electrode and Ag/AgCl (PE-covered silverwire, top dipped in HCl) as reference electrode. The cell was prepared under argon. Tetrabutylammonium hexafluorophosphate (1 mM) was used as electrolyte and acetonitrile as solvent. First cyclic voltametric measurements were performed followed by chronoamperometric measurements (reduction -1.5V , oxidation $+1.5\text{V}$ vs. Ag/AgCl over 600s). The potentials were applied with a PGSTAT 101 Potentiostat from Metrohm. During all measurements simultaneously EPR Spectra were recorded.

UV/vis spectroelectrochemistry. UV/vis absorption spectroelectrochemical spectra were recorded between 250 and 800 nm with an Avantes AvaSpec-2048 UV/vis spectrometer equipped with an AvaLight-DH-S-BAL light source. The compounds were dissolved in acetonitrile and filled into a thin layer quartz cell cuvette with a 1 mm pathlength together with tetrabutylammonium hexafluorophosphate (TBAP, 1 M) which was applied as electrolyte. Prior to the measurements these solutions were purged with argon to work under oxygen free conditions. The working electrode was a platinum mesh (80 mesh, 6x7 mm) and the counter electrode a platinum wire, while a non-aqueous Ag/Ag⁺ electrode (10 mM AgNO₃ in acetonitrile) was applied as reference electrode. The potentials for oxidation ($+1.5$ V), re-reduction (-0.5 V), reduction (-1.5 V) and re-oxidation (0.5 V vs. Ag/Ag⁺) were applied with a PGSTAT 128N Potentiostat from Metrohm. During the redox cycles the potentials were applied for 100 s. The electric charge was checked to be constant at the end of each step.

Photochemical Oxidation and Reduction. The time-dependent absorption spectra of the photochemical oxidation and reduction processes were measured with an Ocean Optics QE65000 spectrometer equipped with a Hamamatsu S7031-1006 detector. As light source for probing a DH-2000 deuterium tungsten halogen lamp with output from 215-2500 nm was applied. The samples were irradiated with light at a wavelength of 350 nm generated by a nanosecond Nd:YAG NT 242 lasersystem from Ekspla. The experiments were performed with methylviologen (2.5 mM) as chemical oxidant and triethylamine (2.5 mM) as chemical reductant.

DFT Calculations. Calculations of the geometries of the copper complex **1** and its oxidized species were performed by using density functional theory with the BP86 functional^{2, 3} and the def2-TZVP basis set.^{4, 5} Frequency calculations were conducted on the optimized geometries in order to verify that the geometries correspond to global minima and that no imaginary frequencies were found. All calculations were carried out using the ORCA 2.9 software package.⁶

Calculations regarding $[\text{Fe}_2(\mu\text{-PPh}_2)(\mu\text{-CO})(\text{CO})_6]^-$ (**3**) have been performed with Gaussian 09⁷ with BP86/def2-TZVP and B₃LYP/6-31+G**⁸⁻¹¹ levels of theory. In both cases two minimum structures with no imaginary frequencies and a very similar absorption pattern of the calculated infrared spectra were found. The calculated frequencies which are shown in Figure S7 have been corrected with a scaling factor of 0.9672 for the B₃LYP/6-31+G** level of theory. This factor is known to be appropriate for such iron cluster anions¹² and is very similar to a factor that was also obtained for a larger set of related molecules.¹³ Frequencies that were obtained from BP86/def2-TZVP calculations have been scaled with a factor of 0.988.¹⁴

Operando FTIR spectroscopy. Measurements were carried out on a Bruker Tensor 27 spectrometer equipped with a mercury-cadmium-telluride (MCT) detector. The optics was purged with nitrogen. The reaction was carried out under argon in a vitreous reaction vessel. The reaction solution was irradiated by a Hg-vapor lamp (Lumatec Superlite 400, 400-700 nm filter) and continuously circulated by a micro gear pump via capillary tubes through an IR-transmission cell (pathlength = 0.1 mm, window material = CaF₂). The reaction temperature was maintained at 25°C with a thermostat. The amount of evolved gas was measured by an automatic gas burette, which was connected to the reaction vessel.

This experimental operando FTIR setup allows for drawing conclusions between activity and the IR-absorption of the catalysts. The pure component spectra and the associated concentration profiles (chapter IR spectra) were extracted with an algorithm based on factor analysis.¹⁵

NMR spectroscopy. NMR spectra were recorded with a Bruker Avance AV-300 (¹H: 300 MHz, ³¹P: 121 MHz) or a Bruker Avance AV-400 (¹H: 400 MHz, ³¹P: 162 MHz) instrument, respectively. The chemical shifts δ are reported in parts per million (ppm) downfield from tetramethylsilane and are referenced to the residual proton resonance of the solvent peak. If not stated otherwise, ³¹P-NMR shifts are proton-decoupled and reported in parts per million downfield from H₃PO₄ and referenced to the signal of PF₆⁻.

Photocatalytic Activity Measurements. All catalytic experiments were carried out under argon atmosphere with freshly distilled solvents. In a standard reaction a double walled and thermostatically controlled reaction vessel was connected to an automatic gas burette. This reactor was several times evacuated and filled with argon to remove any other gases. Subsequently, the copper complexes, Fe₃(CO)₁₂ as well as the Xantphos ligand were introduced in Teflon crucibles. Then the solvent mixture (10 mL), composed of tetrahydrofuran (THF), triethylamine (TEA) and water with a ratio of 4/3/1 (v/v/v), was added and the temperature was maintained at 25 °C by a thermostat. After stirring for approximately 8 min to reach thermal equilibrium the reaction was started by switching on the Xe-lamp (LOT-QuantumDesign, 1.5 W output, without filter). The

amount of the evolved gases was continuously monitored by means of an automatic gas burette and the gas composition was analyzed by gas chromatography (GC). Further details on the equipment and the experimental set-up have been published previously.^{16, 17}

Synthesis of the copper complexes 1 and 2. The copper precursor $[\text{Cu}(\text{MeCN})_4]\text{PF}_6$ and the respective ligands (2,9-dimethyl-4,7-diphenyl-1,10-phenanthroline and Xantphos) were purchased from commercial suppliers and used as received. All reactions were carried out under argon atmosphere using standard Schlenk techniques. Synthesis procedure, NMR spectra, ESI-MS values and elemental analysis of the copper photosensitizers **1** and **2** are similar to those reported earlier in literature.¹⁸⁻²⁰

$[\text{Cu}(\text{2,9-di-methyl-4,7-diphenyl-1,10-phenanthroline})_2]\text{PF}_6$ (**2**): Red solid, 81 % yield. $\text{C}_{52}\text{H}_{40}\text{N}_4\text{CuPF}_6$, $M = 929.41$ g/mol. $^1\text{H-NMR}$ (400 MHz, CDCl_3) δ/ppm : 8.09 (s, 4H), 7.81 (s, 4H), 7.70-7.58 (m, 20H), 2.65 (s, 12H); $^{13}\text{C-NMR}$ (100 MHz, CDCl_3) δ/ppm : 157.3, 149.8, 143.9, 136.8, 129.6, 129.3, 129.0, 125.9, 125.7, 123.9, 26.2; ATR-IR $\tilde{\nu}/\text{cm}^{-1}$: 3052 (w), 2953 (w), 2920 (w), 1619 (w), 1568 (w), 1485 (w), 1439 (w), 830 (s), 750 (m), 700 (s), 556 (s). ESI-HRMS m/z : calculated for $[\text{C}_{52}\text{H}_{40}\text{CuN}_4]^+$: 783.2543; found: 783.2546, $[\text{M}]^+$.

UV/vis spectroelectrochemistry spectra of **1**

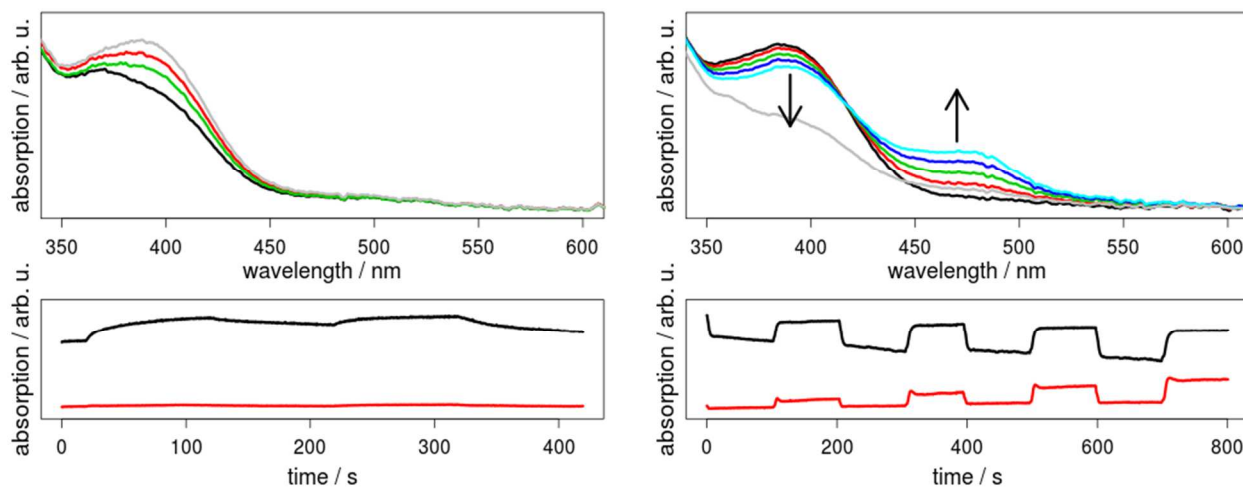


Figure S1. UV/vis absorption spectroelectrochemistry spectra of complex **1** measured in acetonitrile solution.

Left side: The initial spectrum of **1** (black) possesses one absorption band at 390 nm. Afterwards, the electrochemical reduction (-1.5 V) followed by the re-oxidation (+0.5 V vs. Ag/Ag⁺) were carried out. The absorption spectrum during the reduction (grey) and after the whole first (red) and second (green) redox cycle show no changes in the shape of the absorption band. The intensity differences between the cycles can be explained by concentration changes at the platinum mesh. Left side bottom: UV/vis absorption vs. time for two selected wavelengths (390 nm (black) and 480 nm (red)) is shown.

Right side: Another view of the UV/vis spectra of the electrochemical oxidation (+1.5 V) and re-reduction (-0.5 V vs. Ag/Ag⁺) processes compared to the article (Figure 2). The initial spectrum of **1** (black) possesses one absorption band at 390 nm. The spectrum of the oxidized species **1**⁺ without re-reduction is drawn in gray and has a lower absorption in contrast to **1** (compare part O in Figure 2). Subsequently to the oxidation the re-reduction was carried out, and thus, after one (red), two (green), three (blue), and four (cyan) complete redox cycles the band at 390 nm decreases and a new band at higher wavelengths around 475 nm rises. This band can be assigned to the new formed homoleptic CuPS **2** (compare with Figure S2 right, gray spectrum).

Right side bottom: Time traces of the UV/vis absorption for two selected wavelengths (390 nm (black) and 480 nm (red)).

Time-dependent absorption spectra of the photochemical reactions

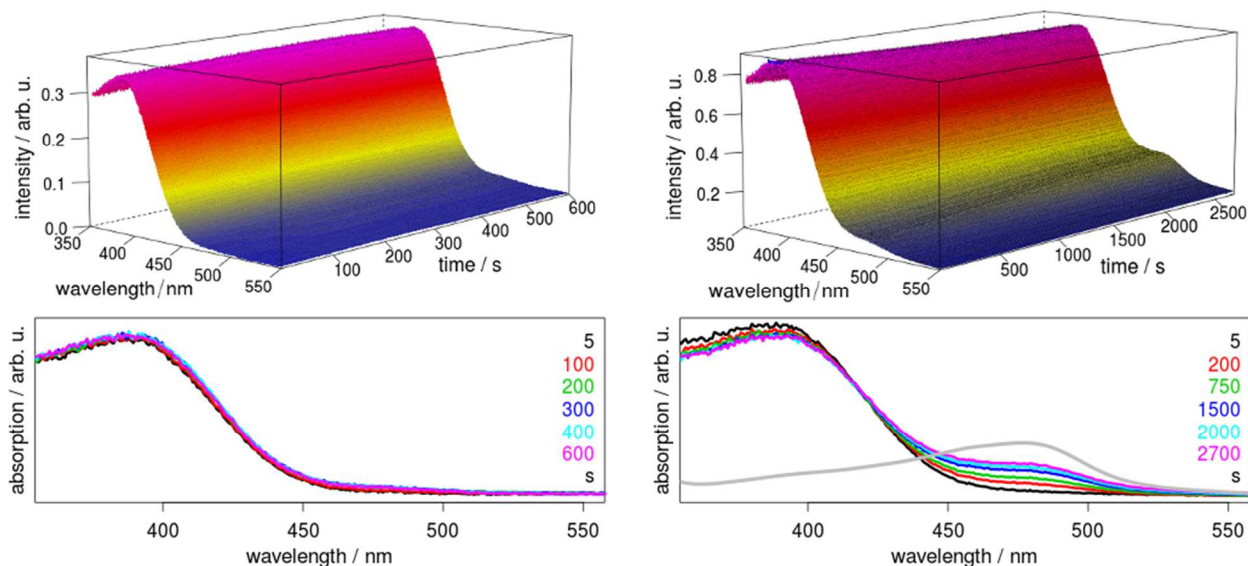


Figure S2. Time-dependent UV/vis absorption spectra of **1** in acetonitrile obtained under continuous excitation at 350 nm.

Left side: Triethylamine was applied as *chemical reductant*. After irradiation with light the excited copper complex $\mathbf{1}^*$ is reduced to $\mathbf{1}^-$ by an electron from the triethylamine electron donor. This electron transfer process from the donor to the photosensitizer (nanosecond time range) and the subsequent recombination (microsecond time range) proceeds very fast compared to the detection time of the absorption spectra (8 ms time resolution). Besides, the reduced species $\mathbf{1}^-$ has a spectrum similar to the initial species **1** (Figure S1 left, gray and black spectrum). Thus, with this method it is not possible to detect the $\mathbf{1}^-$ species itself. Since there are no changes concerning the absorption behavior in the timescale up to 600 s detectable, it is obvious that the reductive electron transfer and recombination processes have no influence on the structure of species **1** and the respective MLCT transitions.

Right side: Methyl viologen dichloride hydrate (MV, 1,1'-dimethyl-4,4'-bipyridinium dichloride in 20% water) was utilized as *chemical oxidant*. In this case the excited copper complex $\mathbf{1}^*$ is oxidized to $\mathbf{1}^+$ by the electron acceptor MV. This electron transfer process from the photosensitizer (nanosecond time range) to MV and the subsequent recombination (microsecond time range) proceeds very fast compared to the detection time of the absorption spectra (8 ms time resolution). Additionally, the oxidized species $\mathbf{1}^+$ itself has a weak absorption intensity in the visible region compared to the initial complex **1** (Figure S1 right, gray and black spectrum). Thus, with this method it is not possible to measure the oxidized species $\mathbf{1}^+$, while the long term changes after oxidation and recombination are detectable. Already after 200 s the formation of a new band at about 475 nm is visible. This new band can be assigned to the homoleptic CuPS **2** as can be seen from the comparison with its absorption spectrum (gray). In overall, the metal-to-ligand charge transfer transition of **1** around 390 nm decreases constantly with increasing time, while a new absorption band at 480 nm appears.

DFT calculations of $\mathbf{1}$, $\mathbf{1}^+$ and $\mathbf{1}^{2+}$

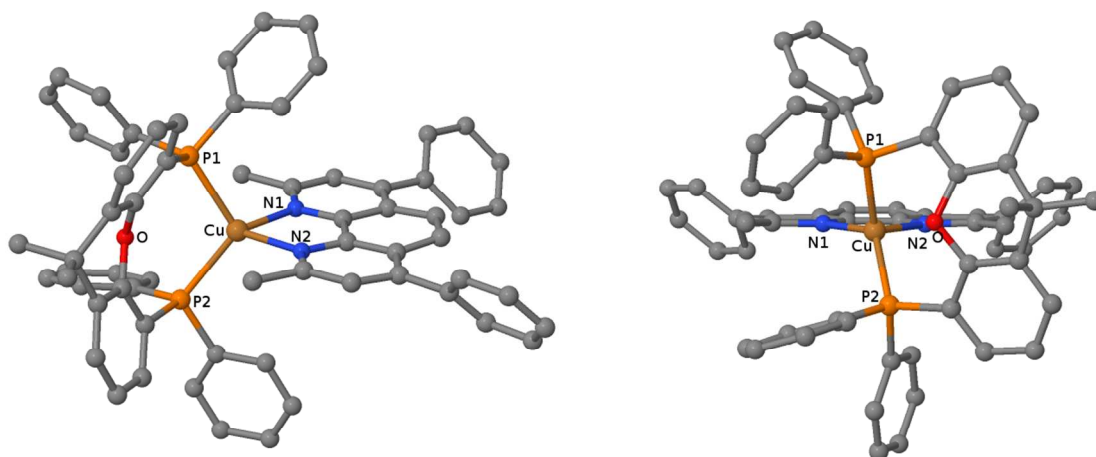


Figure S3. Structure of the ground state of single oxidized copper complex $\mathbf{1}^+$ optimized at the BP86/def2TZVP level of theory (left). Another representation of the structure of $\mathbf{1}^+$ visualizes the spatial twist of the phosphine ligand out of the P-Cu-P plane (right). Hydrogen atoms are omitted for clarity. The Cu (brown), P (orange), N (blue) and O (red) atoms are labeled and the corresponding bond lengths and angles are presented in Table S1.

Table S1. Selected structural data of the copper photosensitizer $\mathbf{1}$, the oxidized $\mathbf{1}^+$ and doubly oxidized $\mathbf{1}^{2+}$ species (compare the labeled atoms with the structure depicted in Figure S3). All data were obtained by DFT calculations (BP86, def2TZVP). The bond lengths are given in nm and the angles in degree. Obviously, the oxidation does not affect the bond lengths and angles of the phenanthroline ligand. Instead, the Cu-P bonds are stepwise enlarged and the P₁-Cu-P₂ angle becomes more acute with increasing oxidation.

bond lengths [nm] and angles [°]	$\mathbf{1}$	$\mathbf{1}^+$	$\mathbf{1}^{2+}$
Cu-N ₁	0.211	0.209	0.210
Cu-N ₂	0.212	0.211	0.212
Cu-P ₁	0.233	0.239	0.241
Cu-P ₂	0.233	0.238	0.239
Cu-O	0.322	0.333	0.338
N ₁ -Cu-N ₂	79.5°	80.4°	79.9°
P ₁ -Cu-P ₂	116.8°	109.2°	103.2°

NMR measurements

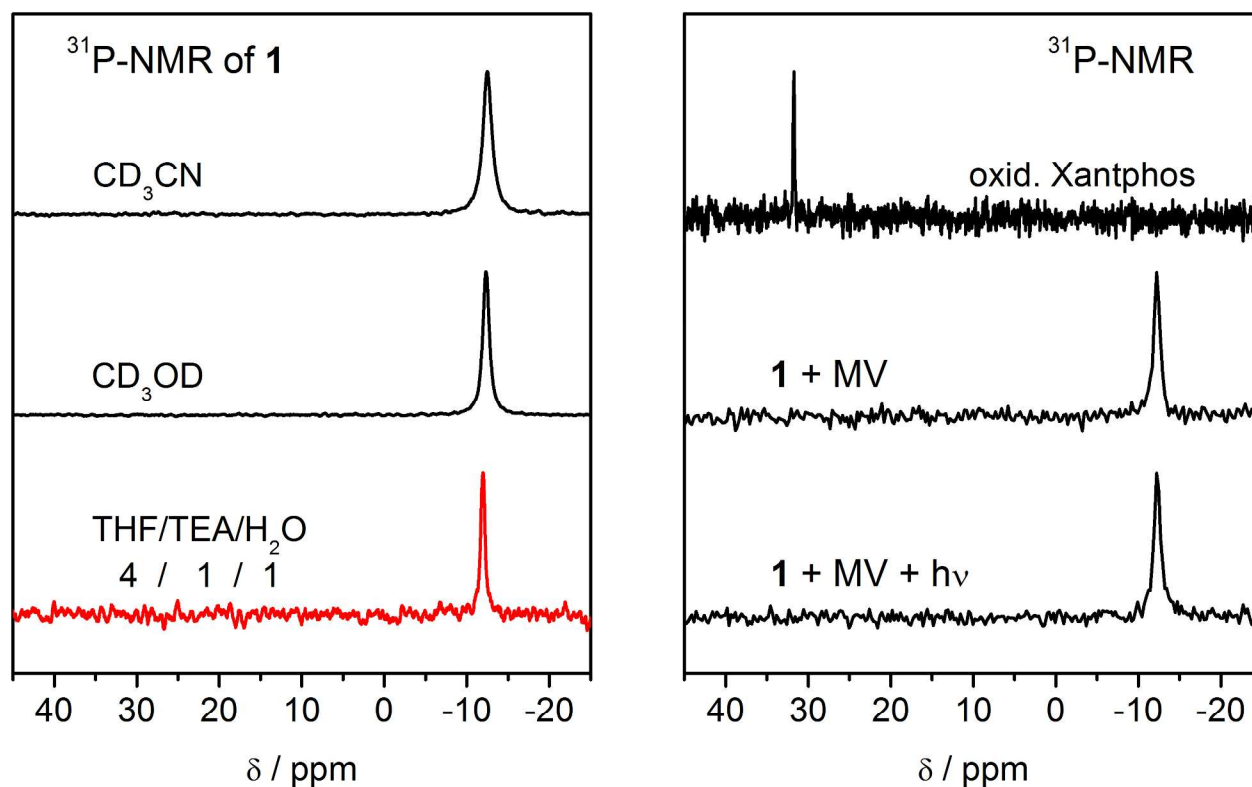


Figure S4. Proton decoupled ^{31}P -NMR spectra of **1** in CD_3CN , CD_3OD or $\text{THF/TEA/H}_2\text{O}$ 4/1/1 (left) and after electrochemical (right, top) as well as photochemical oxidation (right, middle and bottom) in $\text{THF/TEA/H}_2\text{O}$ 4/1/1. The chemical shift of **1** is proven to be independent from the solvent (left). Furthermore, **1** is oxidized electrochemically to Xantphosdioxide (right, top), but not photochemically in the presence of methyl viologen (MV^{2+} , right, middle and bottom).

IR spectra (measured)

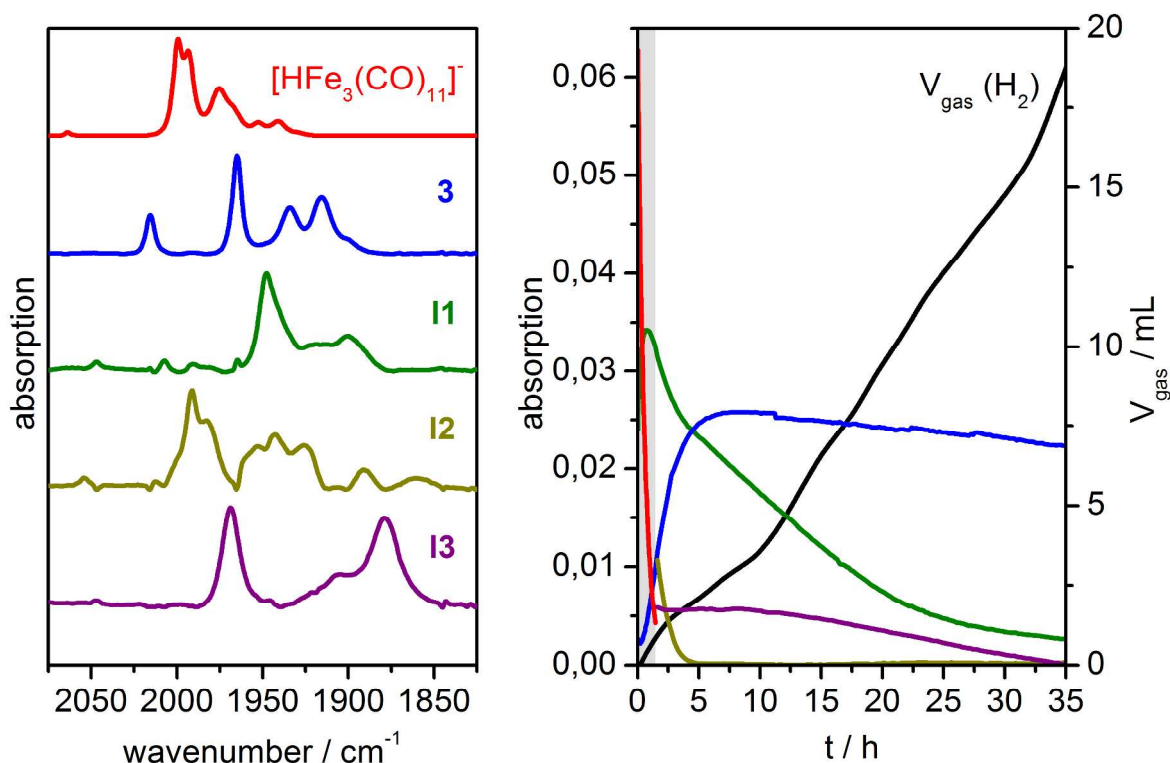


Figure S5. Left: IR-spectra of $[\text{HFe}_3(\text{CO})_{11}]^-$ (red) and $[\text{Fe}_2(\mu\text{-PPH}_2)(\mu\text{-CO})(\text{CO})_6]^-$ (**3**, blue) as well as extracted pure component spectra of the intermediates **I1**, **I2** and **I3** (green, yellow, purple). Right: extracted IR-absorption profiles of the stated species and the respective gas evolution curve (black) during the first 35 h of reaction. The Pure Component Deconvolution (PCD) was realized in two steps. Step 1: 0-1.5 h (highlighted grey) including $[\text{HFe}_3(\text{CO})_{11}]^-$, **3** and **I1**. Step 2: 1.5 – 35 h including **3**, **I1**, **I2** and **I3**. Conditions: 7.0 μmol **1**, 10.0 μmol $[\text{Fe}_3(\text{CO})_{12}]$, 20mL THF/TEA/ H_2O (4/1/1), visible light irradiation (Lumatec Hg-lamp, 1.5W), 25°C.

Table S2. Comparison of selected spectroscopic data of **3** (different cations) with literature.²¹⁻²³

	3 this work	$[(15\text{C}5)\text{Li}]^+ \mathbf{3}^{21}$	$[\text{NEt}_4]^+ \mathbf{3}^{22}$	$[\text{NEt}_4]^+ \mathbf{3}^{22}$	$[\text{PPN}]^+ \mathbf{3}^{23}$
solvent	THF/TEA/ H_2O (4/1/1)	THF	THF	Nujol	Nujol
IR/ cm^{-1}	2015 (m) 1965 (vs) 1934 (m) 1916 (s) 1900 (w,sh) N/A	2015 (ms) 1965 (vs) 1916 (s) 1904 (w, sh)	2010 (m) 1965 (vs) 1935 (s) 1920 (s)	2010 (s) 1965 (s) 1910 (s, br) 1865 (s) 1735 (s, br)	2016 (vs) 1964 (vs, br) 1928 (s) 1904 (w) 1892 (w) 1724 (vs)
NMR ^3P / ppm	126.9 (THF/TEA/ H_2O)	127.0 (CD_3CN)			125.3 (CD_2Cl_2)

s = strong, m = medium, w = weak, vs = very strong, sh = shoulder, br = broad, N/A = not available; $[\text{PPN}]^+$ = bis(triphenylphosphine)iminium cation; $[(15\text{C}5)\text{Li}]^+$ = lithium-15-crown-5 cation.

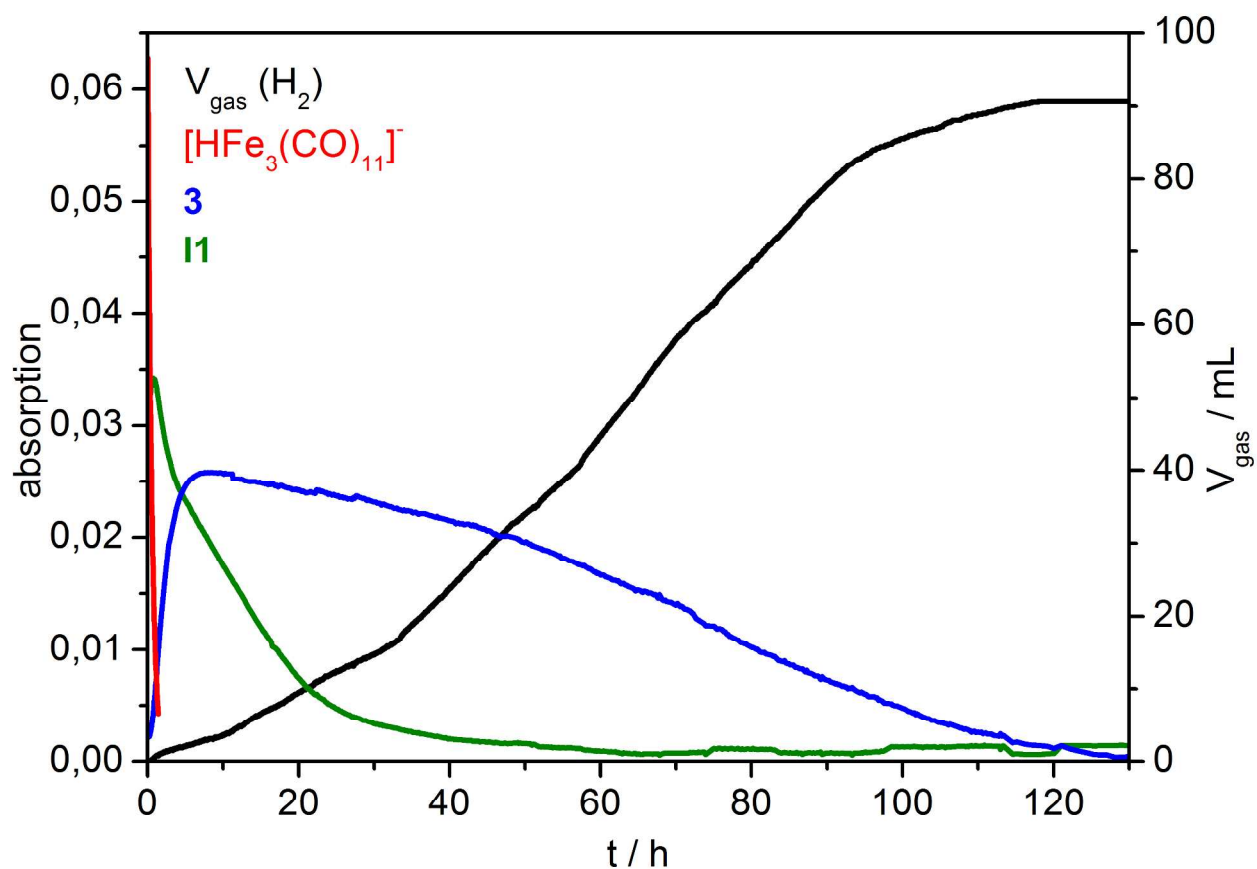


Figure S6. IR-absorption profiles of [HFe₃(CO)₁₁]⁻ (red), [Fe₂(μ-PPh₂)(μ-CO)(CO)₆]⁻ (**3**) (blue) and intermediate **I1** (green) as well as the respective gas evolution curve (black). Conditions: 7.0 μmol CuPS, 10.0 μmol [Fe₃(CO)₁₂], 20mL THF/TEA/H₂O (4/1/1), visible light irradiation (Lumatec Hg-lamp, 1.5W), 25°C; dashed: CuPS **1**; solid: CuPS **2** with 7.0 μmol Xantphos.

IR spectra (calculated)

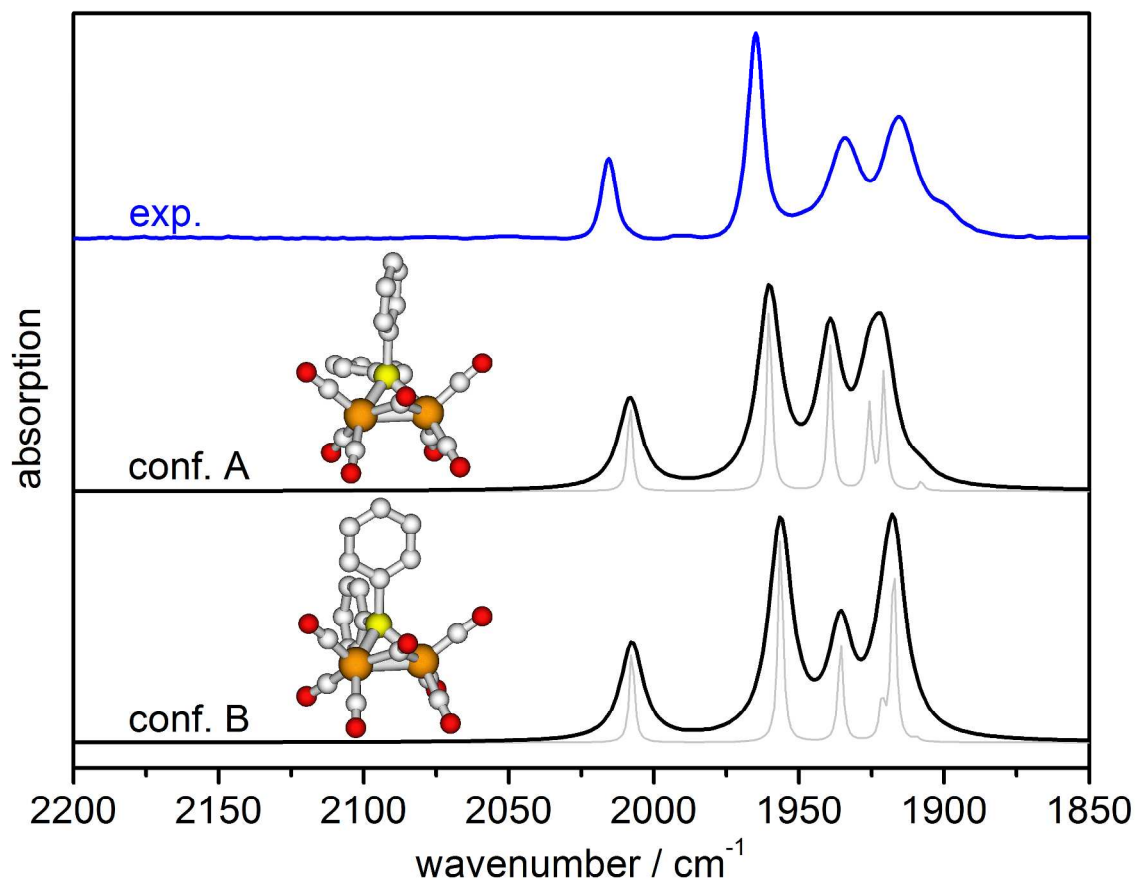


Figure S7. IR spectrum of $[\text{Fe}_2(\mu\text{-PPh}_2)(\mu\text{-CO})(\text{CO})_6]^-$ (**3**): Experiment (top) in comparison with calculations of conformer A (middle) and B (bottom) optimized at the B₃LYP/6-31+G** level of theory. The calculated frequencies were scaled with the factor $f = 0.9672$.¹² Half width = 5 cm⁻¹ (black), half width = 1 cm⁻¹ (grey).

Table S3. Comparison of experimental and calculated frequencies of **3**.

	experiment	B ₃ LYP/6-31+G**		BP86/def2TZVP	
		conf. A	conf. B	conf. A	conf. B
IR/cm ⁻¹	2015 (m)	2008 (m)	2008 (m)	1975 (m)	1974 (m)
	1965 (vs)	1960 (vs)	1956 (vs)	1936 (vs)	1933 (vs)
	1934 (m)	1939 (s)	1935 (m)	1909 (s)	1906 (m)
	1916 (s)	1926 (m), 1921 (s)	1921 (w), 1917 (vs)	1898 (m), 1892 (s)	1889 (vs)
	1900 (w,sh)	1908 (w)	1909 (w)	1882 (w)	-
	N/A	1750 (w)	1759 (w)	1739 (w)	1754 (w)

s = strong, m = medium, w = weak, vs = very strong, sh = shoulder, br = broad, N/A = not available. The experimentally observed contribution at 2015 cm⁻¹ can be assigned to the symmetric stretching mode of all terminal carbonyls whereas the very strong and sharp contribution at 1965 cm⁻¹ represents the corresponding asymmetric stretching mode. The bridged carbonyl ligand could not be detected due to an overlap with the band of acetaldehyde at 1726 cm⁻¹. (Acetaldehyde is formed during the photocatalytic water reduction as a decomposition product of oxidized TEA.)

Photocatalytic experiments

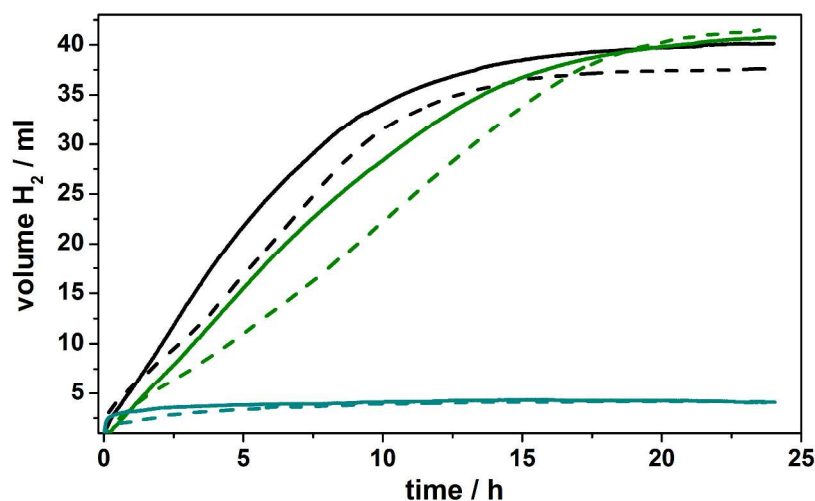


Figure S8. Comparison of the hydrogen evolution curves for the photocatalytic production of hydrogen either using the homoleptic copper photosensitizer **2** (solid lines) or the heteroleptic photosensitizer **1** (dashed lines) with different concentrations in the presence of $[\text{Fe}_3(\text{CO})_{12}]$ ($5.0 \mu\text{mol}$) in a mixture of THF/TEA/ H_2O (10 mL) with the ratio of 4/3/1. Conditions: 1.5 W Xe-light irradiation, without filter, 25°C , 24 h reaction time. The gas evolution was quantitatively measured with automatic gas burettes, while the gas composition was analyzed by GC. Green solid: **2** ($3.5 \mu\text{mol}$) with Xantphos ($3.5 \mu\text{mol}$), green dashed: **1** ($3.5 \mu\text{mol}$) without Xantphos, black solid: **2** ($5.0 \mu\text{mol}$) with Xantphos ($5.0 \mu\text{mol}$), black dashed: **1** ($5.0 \mu\text{mol}$) without Xantphos, grey solid: **2** without Xantphos, grey dashed: only Xantphos ($5.0 \mu\text{mol}$) and $[\text{Fe}_3(\text{CO})_{12}]$.

Table S4. Summary of the photocatalytic experiments and comparison of different concentrations.

entry	CuPS [μmol]	P [^] P [^] ^a [μmol]	$V_{\text{H}_2, \text{max}}$ [ml]	$\text{TON}_{\text{Cu,H}}$ ^b	$\text{TOF}_{5\text{h}}$ [h^{-1}]
1	1 (3.5)	--	39.7	912	49
2	1 (5.0)	--	35.5	572	45
3	2 (3.5)	3.5	39.1	877	77
4	2 (5.0)	5.0	37.5	585	52
5	2 (5.0)	--	4.0 ^c	--	--
6	-- ^d	5.0	4.0	--	--

Conditions: 3.5 or $5.0 \mu\text{mol}$ CuPS, $5.0 \mu\text{mol}$ $[\text{Fe}_3(\text{CO})_{12}]$, in 10 ml THF/TEA/ H_2O (4/3/1), with Xe-lamp (LOT-QuantumDesign, output: 1.5 W, without filter), 25°C , given values are the average of three independent measurements, where the results differ between 5 and 11%.

^a P[^]P[^] = Xantphos (4,5-Bis(diphenylphosphino)-9,9-dimethylxanthene); ^b $\text{TON}_{\text{Cu,H}} = n_{\text{H}}/n_{\text{Cu}}$;

^c represents the blank value of the system; ^d control experiment without CuPS

References

- [1] Petr, A.; Dunsch, L.; Neudeck, A. *J. Electroanal. Chem.* **1996**, *412*, 153-158.
- [2] Becke, A. D. *Phys. Rev. A* **1988**, *38*, 3098-3100.
- [3] Perdew, J. P. *Phys. Rev. B* **1986**, *33*, 8822-8824.
- [4] Schäfer, A.; Horn, H.; Ahlrichs, R. *J. Chem. Phys.* **1992**, *97*, 2571-2577.
- [5] Weigend, F.; Ahlrichs, R. *Phys. Chem. Chem. Phys.* **2005**, *7*, 3297-3305.
- [6] Neese, F. *Wiley Interdiscip. Rev.: Comput. Mol. Sci.* **2012**, *2*, 73-78.
- [7] Frisch, M. J.; Trucks, G. W.; Schlegel, H. B.; Scuseria, G. E.; Robb, M. A.; Cheeseman, J. R.; Scalmani, G.; Barone, V.; Mennucci, B.; Petersson, G. A.; Nakatsuji, H.; Caricato, M.; Li, X.; Hratchian, H. P.; Izmaylov, A. F.; Bloino, J.; Zheng, G.; Sonnenberg, J. L.; Hada, M.; Ehara, M.; Toyota, K.; Fukuda, R.; Hasegawa, J.; Ishida, M.; Nakajima, T.; Honda, Y.; Kitao, O.; Nakai, H.; Vreven, T.; Montgomery, J. A., Jr.; Peralta, J. E.; Ogliaro, F.; Bearpark, M.; Heyd, J. J.; Brothers, E.; Kudin, K. N.; Staroverov, V. N.; Kobayashi, R.; Normand, J.; Raghavachari, K.; Rendell, A.; Burant, J. C.; Iyengar, S. S.; Tomasi, J.; Cossi, M.; Rega, N.; Millam, N. J.; Klene, M.; Knox, J. E.; Cross, J. B.; Bakken, V.; Adamo, C.; Jaramillo, J.; Gomperts, R.; Stratmann, R. E.; Yazyev, O.; Austin, A. J.; Cammi, R.; Pomelli, C.; Ochterski, J. W.; Martin, R. L.; Morokuma, K.; Zakrzewski, V. G.; Voth, G. A.; Salvador, P.; Dannenberg, J. J.; Dapprich, S.; Daniels, A. D.; Farkas, Ö.; Foresman, J. B.; Ortiz, J. V.; Cioslowski, J.; Fox, D. J., *Gaussian 09, Revision D.01*. Gaussian, Inc., Wallingford CT, 2009.
- [8] Becke, A. D. *J. Chem. Phys.* **1993**, *98*, 5648-5652.
- [9] Lee, C.; Yang, W.; Parr, R. G. *Phys. Rev. B* **1988**, *37*, 785-789.
- [10] McLean, A. D.; Chandler, G. S. *J. Chem. Phys.* **1980**, *72*, 5639-5648.
- [11] Krishnan, R.; Binkley, J. S.; Seeger, R.; Pople, J. A. *J. Chem. Phys.* **1980**, *72*, 650-654.
- [12] Chi, C.; Cui, J.; Li, Z. H.; Xing, X.; Wang, G.; Zhou, M. *Chem. Sci.* **2012**, *3*, 1698-1706.
- [13] Irikura, K. K.; Johnson, R. D.; Kacker, R. N. *J. Phys. Chem. A* **2005**, *109*, 8430-8437.
- [14] Alecu, I. M.; Zheng, J.; Zhao, Y.; Truhlar, D. G. *J. Chem. Theory Comput.* **2010**, *6*, 2872-2887.
- [15] Neymeyr, K.; Sawall, M.; Hess, D. *J. Chemometrics* **2010**, *24*, 67-74.
- [16] Gärtner, F.; Boddien, A.; Barsch, E.; Fumino, K.; Losse, S.; Junge, H.; Hollmann, D.; Brueckner, A.; Ludwig, R.; Beller, M. *Chem. Eur. J.* **2011**, *17*, 6425-6436.
- [17] Gärtner, F.; Losse, S.; Boddien, A.; Pohl, M.-M.; Denurra, S.; Junge, H.; Beller, M. *ChemSusChem* **2012**, *5*, 530-533.
- [18] Kuchiyama, Y.; Kobayashi, N.; Takagi, H. D. *Inorg. Chim. Acta* **1998**, *277*, 31-36.
- [19] Luo, S.-P.; Mejía, E.; Friedrich, A.; Pazidis, A.; Junge, H.; Surkus, A.-E.; Jackstell, R.; Denurra, S.; Gladiali, S.; Lochbrunner, S.; Beller, M. *Angew. Chem. Int. Ed.* **2013**, *52*, 419-423.
- [20] Mejía, E.; Luo, S.-P.; Karnahl, M.; Friedrich, A.; Tschierlei, S.; Surkus, A.-E.; Junge, H.; Gladiali, S.; Lochbrunner, S.; Beller, M. *Chem. Eur. J.* **2013**, *19*, 15972-15978.
- [21] Cheah, M. H.; Borg, S. J.; Bondin, M. I.; Best, S. P. *Inorg. Chem.* **2004**, *43*, 5635-5644.
- [22] Ellis, J. E.; Chen, Y. S. *Organometallics* **1989**, *8*, 1350-1361.
- [23] Walther, B.; Hartung, H.; Böttcher, H.-C.; Baumeister, U.; Böhland, U.; Reinhold, J.; Sieler, J.; Ladriere, J.; Schiebel, H.-M. *Polyhedron* **1991**, *10*, 2423-2435.